NIH Public Access
Author Manuscript
Biochemistry. Author manuscript; available in PMC 2008 June 12.

Published in final edited form as:
Biochemistry. 2004 May 11; 43(18): 5138–5148.

Poliovirus RNA-Dependent RNA Polymerase (3D^{pol}):

Pre-Steady-State Kinetic Analysis of Ribonucleotide Incorporation in the Presence of Mn^{2+}Δ

Jamie J. Arnold, **David W. Gohara**‡, and **Craig E. Cameron***
Department of Biochemistry and Molecular Biology, The Pennsylvania State University, University Park, Pennsylvania 16802

Abstract

The use of Mn^{2+} as the divalent cation cofactor in polymerase-catalyzed reactions instead of Mg^{2+} often diminishes the stringency of substrate selection and incorporation fidelity. We have solved the complete kinetic mechanism for single nucleotide incorporation catalyzed by the RNA-dependent RNA polymerase from poliovirus (3D^{pol}) in the presence of Mn^{2+}. The steps employed during a single cycle of nucleotide incorporation are identical to those employed in the presence of Mg^{2+} and include a conformational-change step after nucleotide binding to achieve catalytic competence of the polymerase-primer/template-nucleotide complex. In the presence of Mn^{2+}, the conformational-change step is the primary determinant of enzyme specificity, phosphoryl transfer appears as the sole rate-limiting step for nucleotide incorporation, and the rate of phosphoryl transfer is the same for all nucleotides: correct and incorrect. Because phosphoryl transfer is the rate-limiting step in the presence of Mn^{2+}, it was possible to determine that the maximal phosphorothioate effect in this system is in the range of 8-11. This information permitted further interrogation of the nucleotide-selection process in the presence of Mg^{2+}, highlighting the capacity of this cation to permit the enzyme to use the phosphoryl-transfer step for nucleotide selection. The inability of Mn^{2+} to support a reduction in the efficiency of phosphoryl transfer when incorrect substrates are employed is the primary explanation for the loss of fidelity observed in the presence of this cofactor. We propose that the conformational change involves reorientation of the triphosphate moiety of the bound nucleotide into a conformation that permits binding of the second metal ion required for catalysis. In the presence of Mg^{2+}, this conformation requires interactions with the enzyme that permit a reduction in catalytic efficiency to occur during an attempt to incorporate an incorrect nucleotide. Adventitious interactions in the cofactor-binding site with bound Mn^{2+} may diminish fidelity by compensating for interaction losses used to modulate catalytic efficiency when incorrect nucleotides are bound in the presence of Mg^{2+}.

All nucleic acid polymerases require two divalent cations as cofactors to catalyze phosphoryl transfer (1). The first metal ion is brought into the active site complexed to the triphosphate moiety of the nucleotide substrate. This metal ion may facilitate formation of the conformation of the triphosphate required for nucleophilic attack of the α-phosphorus atom. The second metal ion is required to lower the pK_a of the primer 3′-OH to facilitate formation of the nucleophile required for catalysis. Mg^{2+} is thought to be the divalent cation employed by most polymerases known (2); however, activity is usually supported by other divalent cations as well (3-7). In a

Δ This work was supported, in part, by a Howard Temin Award (CA75118) from the NCI, National Institutes of Health, and by a grant (AI45818) from the NIAID, National Institutes of Health (both to C.E.C.). C.E.C. is the recipient of an Established Investigator Award (0340028N) from the American Heart Association.

* To whom correspondence should be addressed. Tel: 814-863-8705. Fax: 814-865-7927. E-mail: cec9@psu.edu.
‡ Present address: Department of Biological Chemistry and Molecular Pharmacology, Harvard Medical School, 240 Longwood Ave., Boston, MA 02115.

NIH-PA Author Manuscript
NIH-PA Author Manuscript
NIH-PA Author Manuscript

NIH-PA Author Manuscript

NIH-PA Author Manuscript

NIH-PA Author Manuscript

variety of polymerase systems, Mn^{2+} has been shown to be an effective divalent cation cofactor (3-7). However, this metal usually alters the biochemical properties of the polymerase, decreasing the stringency of substrate selection and incorporation fidelity (4,5,7-10). Despite years of effort, neither steady-state kinetic nor structural studies have yielded any significant insight into the mechanistic or molecular basis for the destructive effects of Mn^{2+} on polymerase fidelity.

Our studies of the RNA-dependent RNA polymerase (RdRP)[1] from poliovirus ($3D^{pol}$) have shown that replacement of the Mg^{2+} cofactor with Mn^{2+} alters the biochemical properties of this enzyme, permitting increased use of DNA templates, nucleotides with incorrect sugar configurations (e.g., 2′-dNTPs, 3′-dNTPs, and 2′,3′-ddNTPs), and nucleotides with incorrect

---

[1]Abbreviations:

RdRP RNA-dependent RNA polymerase

2′-dNTP 2′-deoxynucleoside 5′-triphosphate

3′-dNTP 3′-deoxynucleoside 5′-triphosphate

2′,3′-ddNTP 2′,3′-dideoxynucleoside 5′-triphosphate

ATP adenosine 5′-triphosphate

NTP nucleoside 5′-triphosphate

EDTA ethylenediaminetetraacetic acid

PAGE polyacrylamide gel electrophoresis

AMP adenosine 5′-monophosphate

2′-dAMP 2′-deoxyadenosine 5′-monophosphate

UMP uridine 5′-monophosphate

GMP guanosine 5′-monophosphate

PP_i pyrophosphate

ATPαS adenosine 5′-*O*-(1-thiotriphosphate)

2′-dATPαS 2′-deoxyadenosine 5′-*O*-(1-thiotriphosphate)

GTPαS guanosine 5′-*O*-(1-thiotriphosphate)

2′-dATP 2′-deoxyadenosine 5′-triphosphate

GTP guanosine 5′-triphosphate.

NIH-PA Author Manuscript

NIH-PA Author Manuscript

NIH-PA Author Manuscript

bases (7). Recently, we developed the tools to characterize the complete kinetic mechanism for single nucleotide incorporation catalyzed by $3D^{pol}$ (11). We have shown that in the presence of Mg^{2+} this enzyme employs the same overall kinetic mechanism as reported for other nucleic acid polymerases (12). Nucleotide binds to the polymerase-primer/template complex. This ternary complex isomerizes into a catalytically competent complex. Phosphoryl transfer occurs followed by a second conformational change, perhaps translocation, and pyrophosphate release (12).

Despite the availability of complete kinetic mechanisms for single nucleotide incorporation in the presence of Mg^{2+} for a variety of polymerases (13-17), comparable data do not exist for nucleotide incorporation in the presence of Mn^{2+}. We have filled this gap by elucidating the complete kinetic mechanism for $3D^{pol}$-catalyzed single nucleotide incorporation in the presence of Mn^{2+}. These studies have permitted us not only to develop a complete kinetic and thermodynamic understanding for correct and incorrect nucleotide incorporation in the presence of Mn^{2+} but also to expand our kinetic and thermodynamic appreciation for incorrect nucleotide incorporation in the presence of Mg^{2+}. Succinctly, we find that, by using Mg^{2+} as the divalent cation cofactor, $3D^{pol}$ can use both the first conformational-change step and the phosphoryl-transfer step to distinguish between correct and incorrect nucleotides. However, by using Mn^{2+} as the cofactor, the ability to diminish the rate of phosphoryl transfer for incorrect nucleotides relative to correct nucleotides is lost completely, leaving only the conformational-change step for selection of the correct nucleotide. We discuss these results in the context of our structural model for the $3D^{pol}$ ternary complex (18).

EXPERIMENTAL PROCEDURES

Materials

[γ-^{32}P]ATP (>7000 Ci/mmol) was from ICN; [α-^{32}P]ATP (3000 Ci/mmol) was from New England Nuclear; nucleoside 5′-triphosphates, 2′-deoxynucleoside 5′-triphosphates (all nucleotides were ultrapure solutions), adenosine 5′-*O*-(1-thiotriphosphate) (ATPαS), and 2′-deoxyadenosine 5′-*O*-(1-thiotriphosphate) (2′-dATPαS) were from Amersham Pharmacia Biotech, Inc. Guanosine 5′-*O*-(1-thiotriphosphate) (GTPαS) was from TriLink Biotechnologies; all RNA oligonucleotides were from Dharmacon Research, Inc. (Boulder, CO); T4 polynucleotide kinase was from New England Biolabs, Inc.; sodium pyrophosphate was from American Bioanalytical; all other reagents were of the highest grade available from Sigma, Fisher, or VWR.

Expression and Purification of $3D^{pol}$

Expression and purification of $3D^{pol}$ were performed as described previously (19).

Purification, 5′-^{32}P Labeling, and Annealing of sym/sub

RNA oligonucleotides were purified, labeled, and annealed as described previously (11).

$3D^{pol}$ Assays

Reactions contained 50 mM HEPES, pH 7.5, 10 mM 2-mercaptoethanol, 5 mM $MnCl_2$, 60 μM $ZnCl_2$, nucleotide, sym/sub, and $3D^{pol}$. Reactions were performed at 30 °C. $3D^{pol}$ was diluted immediately prior to use in 50 mM HEPES, pH 7.5, 10 mM 2-mercaptoethanol, 60 μM $ZnCl_2$, and 20% glycerol. Zn^{2+} was added to increase the stability of the enzyme; however, the level of Zn^{2+} employed is insufficient to support nucleotide incorporation. The volume of enzyme added to any reaction was always less than or equal to one-tenth the total volume. Reactions were quenched by addition of EDTA to a final concentration of either 50 mM or 0.3 M or by addition of HCl to a final concentration of 1 M. Immediately after the addition of HCl,

NIH-PA Author Manuscript

NIH-PA Author Manuscript

NIH-PA Author Manuscript

the solution was neutralized by addition of 1 M KOH and 300 mM Tris (final concentration). Specific concentrations of primer/template and $3D^{pol}$, along with any deviations from the above, are indicated in the appropriate figure legend.

Rapid Chemical-Quench-Flow Experiments

Rapid mixing/quenching experiments were performed by using a Model RQF-3 chemical-quench-flow apparatus (KinTek Corp., Austin, TX). Experiments were performed at 30 °C by using a circulating water bath. $3D^{pol}$-sym/sub complexes were assembled by mixing $3D^{pol}$ and sym/sub for 3 min at room temperature and then rapidly mixed with the nucleotide substrate. After mixing, reactant concentrations were reduced by 50%. Reactions were quenched either by addition of EDTA to a final concentration of 0.3 M or by addition of HCl to a final concentration of 1 M. Immediately after the addition of HCl, the solution was neutralized by addition of 1 M KOH and 300 mM Tris (final concentration).

Product Analysis: Denaturing PAGE

An equal volume of loading buffer (90% formamide, 0.025% bromophenol blue, and 0.025% xylene cyanol) was added to 10 μL of the quenched reaction mixtures and heated to 70 °C for 2-5 min prior to loading 5 μL on a denaturing 23% polyacrylamide gel containing 1× TBE and 7 M urea. Electrophoresis was performed in 1× TBE at 90 W. Gels were visualized by using a phosphorimager and quantified by using the ImageQuant software (Molecular Dynamics).

Data Analysis

Data were fit by nonlinear regression using the program KaleidaGraph (Synergy Software, Reading, PA). Time courses at fixed nucleotide concentration were fit to

$$[\text{product}] = Ae^{-k_{obs}t} + C \quad (1)$$

where A is the amplitude of the burst, k_{obs} is the observed first-order rate constant describing the burst, t is the time, and C is a constant. The apparent binding constant ($K_{d,app}$) and maximal rate constant for nucleotide incorporation (k_{pol}) were determined using the equation:

$$k_{obs} = \frac{k_{pol}[\text{NTP}]}{K_{d,app} + [\text{NTP}]} \quad (2)$$

The value for the equilibrium constant across the conformational-change step was determined using the equations (17):

$$k_{chem} = k_{pol}\Lambda_2\frac{\sigma - 1}{E_{obs} - 1} \quad (3)$$

$$K_2 = \frac{1}{\Lambda_2 - 1} \quad (4)$$

$$K_2 = \frac{k_{+2}}{k_{-2}} \quad (5)$$

k_{chem} is the rate constant for the chemical step (referred to as k_{+3} throughout), k_{pol} is the maximal observed rate constant for nucleotide incorporation, σ is the maximal elemental effect, E_{obs} is the observed elemental effect, and k_{+2} and k_{-2} are the forward and reverse rate constants for the conformational-change step, respectively (see Scheme 1).

NIH-PA Author Manuscript

NIH-PA Author Manuscript

NIH-PA Author Manuscript

Kinetic Simulation

Kinetic simulations were performed by using KinTekSim Version 2.03 (KinTek Corp., Austin, TX). All rate constants were determined experimentally, except where noted. The agreement between the experimental data and kinetic simulations was determined by visual inspection.

RESULTS

3D^{pol}-Catalyzed Nucleotide Incorporation in the Presence of Mn^{2+}

The goal of this study was to determine the mechanistic basis for differences observed in the efficiency and specificity of 3D^{pol}-catalyzed nucleotide incorporation when the divalent cation cofactor is changed from Mg^{2+} to Mn^{2+} (7). These studies employed the symmetrical primer/template system developed to study this enzyme (11). Each primer/template will be referred to as sym/sub; if the templating base was uracil, for example, then this substrate was designated sym/sub-U. It is also worth noting that 3D^{pol}-sym/sub complexes are very stable, having a half-life of approximately 2 h at 25 °C. Consequently, neither binding nor dissociation of sym/sub needs to be considered in our interpretation of the kinetic experiments described herein.

To perform the kinetic experiments, 3D^{pol}-sym/sub-U complexes were formed in the presence of either Mg^{2+} or Mn^{2+}, rapidly mixed with ATP, the correct nucleotide, and quenched at various times by addition of EDTA. In the presence of Mn^{2+}, the observed kinetics of nucleotide incorporation were biphasic (Figure 1A, filled circles), while in the presence of Mg^{2+}, the kinetics of nucleotide incorporation were monophasic (Figure 1B, filled circles). The biphasic nature of the time course observed in the presence of Mn^{2+} was not altered by quenching as fast as possible (2 ms). These data were consistent with the formation of an intermediate (e.g., *ER$_n$NTP in Scheme 1) in the presence of Mn^{2+} that could not be quenched by using EDTA. Clearly, in order for EDTA to be an effective quench, at least one of the metals required for catalysis must dissociate rapidly relative to chemistry. Because protons can enter into the productive 3D^{pol}-sym/sub-U-ATP complex, acid might be a better quenching agent. As shown in Figure 1A (open circles), by using an acid quench, the kinetics of nucleotide incorporation were now monophasic in the presence of Mn^{2+}. Importantly, the observed kinetics of nucleotide incorporation were not altered when Mg^{2+} was employed as the divalent cation cofactor and acid was employed as the quench (Figure 1B).

The end-point values differed between experiments performed in the presence of Mn^{2+} and Mg^{2+} (cf. panels A and B of Figure 1). This difference is due to an increase in the concentration of the 3D^{pol}-sym/sub complex formed when Mn^{2+} is employed (11). In addition, the observed rate constant for nucleotide incorporation was decreased from $43 \pm 3 s^{-1}$ in the presence of Mg^{2+} to $21 \pm 1 s^{-1}$ in the presence of Mn^{2+}. The observation of a decreased rate constant for correct nucleotide incorporation for wild-type 3D^{pol} in the presence of Mn^{2+} relative to Mg^{2+} differs from previously reported observations and is a reflection of the use of an EDTA quench in that study (18).

Solution of the Complete Kinetic Mechanism for Correct Nucleotide Incorporation in the Presence of Mn^{2+}

Scheme 1 shows the complete kinetic mechanism for 3D^{pol}-catalyzed AMP incorporation into sym/sub-U determined in the presence of Mg^{2+} (12). Nucleotide binds to the enzyme-primer/template complex (step 1), this complex isomerizes (step 2), phosphoryl transfer occurs (step 3) followed by a second conformational change, perhaps translocation (step 4), and pyrophosphate release (step 5). While Mn^{2+} likely impacts one or more of these steps, we considered it unlikely that Mn^{2+} causes a change in the number or nature of steps employed by the enzyme for nucleotide incorporation (12).

NIH-PA Author Manuscript

NIH-PA Author Manuscript

NIH-PA Author Manuscript

First, we evaluated the concentration dependence of AMP incorporation into sym/sub-U (Figure 2A). The observed rate constant for nucleotide incorporation was determined for each concentration of nucleotide employed by fitting the data to the equation describing a single exponential (eq 1; data not shown). By plotting the observed rate constant as a function of ATP concentration, we obtained values of 4.1 ± 0.5 μM and 21.4 ± 0.6 s^{-1} for $K_{d,app}$ and k_{pol}, respectively. Relative to the values measured in the presence of Mg^{2+}, the $K_{d,app}$ value decreased by 30-fold and the k_{pol} value decreased by 4-fold (12). The apparent increase in affinity for the correct nucleotide and/or decrease in overall rate of incorporation were (was) not unique to the experiment described above as incorporation of UMP into sym/sub-UA and incorporation of GMP into sym/sub-C showed the same trends (Table 1). These data are consistent with Mn^{2+} having some effect on steps 1-3 of the mechanism.

To interrogate steps 2 and 3 more directly, we performed pulse-quench and pulse-chase experiments (Figure 3A). In these experiments, the $3D^{pol}$-sym/sub complex is mixed with [α-^{32}P]ATP for various amounts of time and then either quenched or chased by addition of ATP and then quenched. If the intermediate described in step 2 of Scheme 1 exists in the presence of Mn^{2+}, then the pulse-chase experiment should show additional product relative to the pulse-quench experiment because the chase period permits a fraction of the isomerized complex to be converted to product complex (12). The data obtained from these experiments are shown in Figure 3B. The data are consistent with the existence of a conformational change preceding phosphoryl transfer. Kinetic simulation was used to fit the data to the mechanism shown in Scheme 2 (data not shown). These data yielded a limit of 3 for the value of K_2 (k_{+2}) = 300-1500 s^{-1}; k_{-2}) = 100-500 s^{-1}) and a value of 30 s^{-1} for k_{+3}, the rate constant for phosphoryl transfer. From these data, it is possible to conclude that Mn^{2+} increases the overall stability of the isomerized complex by a factor of 5 and decreases the rate of phosphoryl transfer by a factor of 17 relative to the values measured/modeled in the presence of Mg^{2+}. In addition, in the presence of Mn^{2+}, phosphoryl transfer is the sole rate-limiting step for correct nucleotide incorporation.

If phosphoryl transfer is the rate-limiting step in the presence of Mn^{2+}, then the observed phosphorothioate effect should be greater than the value of 4.2 observed in the presence of Mg^{2+} (Table 2) (12). In fact, the phosphorothioate effect measured for a given nucleotide substrate in the presence of Mn^{2+} should reflect the theoretical maximum for that substrate. As shown in Figure 4 for 100 μM ATP or ATPαS, the observed phosphorothioate effect was 7.6. This value increased to 7.9 ± 0.4 when values for k_{pol} were employed (Tables 1 and 2). A value of 8.2 ± 0.6 was determined for the phosphorothioate effect when GTP/GTPαS was evaluated (Tables 1 and 2). These values are in good agreement with the range of 4-11 reported by Herschlag, Piccirilli, and Cech in their evaluation of the phosphorothioate effects in nonenzymatic reactions (20).

In the presence of Mg^{2+}, phosphoryl transfer can be run in reverse [pyrophosphorolysis and pyrophosphate exchange (12)]; however, this is not the case when Mn^{2+} is employed as the divalent cation cofactor (data not shown). Evaluation of the reverse reaction rate permits determination of the $K_{d,app}$ value for PP_i and estimation of rate constants for the conformational-change step after nucleotide incorporation, thereby completing the mechanism (12).

In the presence of Mg^{2+}, the rate-limiting step for consecutive cycles of nucleotide incorporation is likely the conformational change after nucleotide incorporation (12). Experimentally, this conclusion was reached by kinetic simulation of two successive cycles of nucleotide incorporation and comparison of the simulated data to that derived from empirical analysis of single nucleotide incorporation (12). We performed a similar experiment in the presence of Mn^{2+} (Figure 5A). The data were simulated to the simple mechanism shown in

NIH-PA Author Manuscript

NIH-PA Author Manuscript

NIH-PA Author Manuscript

Scheme 3 using the appropriate constants from Table 1 (data not shown). The kinetic simulation set a lower limit of 160 s^{-1} on the rate constant for the second conformational change (k_{+4}). The upper limit of 1.0×10^{-4} s^{-1} for k_{-4} was constrained by the fact that greater values should produce detectable levels of ATP in the pyrophosphorolysis experiment over the 10000 s time period monitored. By performing this experiment in the presence of pyrophosphate, we were able to estimate a K_d value of 200 μM for pyrophosphate by evaluating the capacity of pyrophosphate to inhibit the second cycle of nucleotide incorporation (Figure 5B). Together, these studies permit us to conclude that the primary effect of Mn^{2+} on correct nucleotide incorporation is a 5-fold increase in the equilibrium constant for the conformational-change step preceding phosphoryl transfer and a 17-fold decrease in the rate constant for phosphoryl transfer.

Effect of Mn^{2+} on Fidelity of $3D^{pol}$-Catalyzed Nucleotide Incorporation

We have used 2′-dATP and GTP to evaluate the mechanism employed by $3D^{pol}$ to distinguish between nucleotides containing an incorrect sugar configuration or an incorrect base, respectively. The concentration dependence of the kinetics of 2′-dAMP or GMP incorporation into sym/sub-U was evaluated, and these data were used to determine values for $K_{d,app}$ and k_{pol} (data not shown; Table 1). In both cases, the $K_{d,app}$ values decreased, and the k_{pol} values increased relative to the corresponding values measured in the presence of Mg^{2+} (Table 1). The $K_{d,app}$ value for 2′-dATP decreased 15-fold to 19.2 ± 4.0 μM, and the value for GTP decreased 2-fold to 173 ± 20 μM (Table 1). The k_{pol} value for 2′-dATP increased 11-fold to 8.5 ± 0.6 s^{-1}, and the value for GTP increased 131-fold to 1.7 ± 0.1 s^{-1}. These changes correspond to an overall 18-fold reduction in the ability of $3D^{pol}$ to select the correct sugar configuration and to an overall 29-fold reduction in the ability of $3D^{pol}$ to select the correct base when Mn^{2+} is substituted for Mg^{2+} (Table 3).

Mechanistic Basis for the Loss of $3D^{pol}$ Fidelity in the Presence of Mn^{2+}

Because both the conformational change preceding phosphoryl transfer and phosphoryl transfer were affected most by the divalent cation substitution, these steps were most likely to be involved in fidelity of nucleotide selection. Therefore, we evaluated 2′-dAMP and GMP incorporation by using an EDTA quench. As demonstrated for AMP incorporation, this experiment can serve as a surrogate for the pulse-chase experiment, and the resulting data are modeled well by Scheme 2 (cf. Figures 6A and 3B). The constants obtained by using ATP set upper limits for K_2 (3) and k_{+3} (30 s^{-1}). For both 2′-dATP and GTP, the EDTA-quench data were modeled best by conditions in which K_2 changed without affecting k_{+3} (filled circles and solid lines in Figure 6B,C). If k_{+3} functioned as the sole step mediating enzyme fidelity, then a significant quantity of EDTA-resistant intermediate should accumulate with both 2′-dATP and GTP (dashed lines in Figure 6B,C). Clearly, this was not observed. The K_2 value for 2′-dATP was 0.4, and that for GTP was 0.05 (Table 4). These experiments could not attribute the change in K_2 specifically to a decrease in k_{+2}, an increase in k_{-2}, or some combination thereof relative to data obtained for ATP.

The value for K_2 can also be calculated by using the combination of eqs 3-5. This calculation requires knowledge of the values for the theoretical/maximal phosphorothioate effect and the observed phosphorothioate effect. We assumed that chemistry was completely rate limiting for 2′-dAMP incorporation so a value of 11 was used as both the theoretical maximum and observed phosphorothioate effect (Tables 1 and 2), yielding a K_2 value of 0.4, which is in perfect agreement with that obtained by simulation of the EDTA-quench experiment (Table 4 and Figure 6B). For GMP incorporation, we assumed that the phosphorothioate effect of 8.2 determined for GTP/GTPαS as a correct nucleotide would set an upper limit on the phosphorothioate effect for GTP/GTPαS incorporation as an incorrect nucleotide; the empirically determined value for GTP/GTPαS as an incorrect nucleotide was 5.7 (Tables 1 and

NIH-PA Author Manuscript

NIH-PA Author Manuscript

NIH-PA Author Manuscript

2). The calculated K_2 value was 0.10, which is in good agreement with that obtained by simulation of the EDTA-quench experiment (Table 4 and Figure 6C). Together, these data permit us to conclude that in the presence of Mn^{2+} the conformational-change step preceding chemistry is the primary step used for nucleotide selection.

Mechanistic Basis for 3D^{pol} Fidelity in the Presence of Mn^{2+}

Given a value for K_2 and the appropriate information for theoretical and observed phosphorothioate effects, we can calculate a value for k_{+3} by using eqs 3-5. Having values for K_2 and k_{+3} will permit a complete kinetic description of the nucleotide-selection process in the presence of Mg^{2+}. The Mn^{2+} data fill important gaps by permitting this missing information to be obtained (12). To estimate the value of K_2 in the presence of Mg^{2+} for 2′-dAMP and GMP incorporation into sym/sub-U, we used the following logic. The ratio of $K_{2,ATP,Mn^{2+}}/K_{2,ATP,Mg^{2+}}$ (a value of 5) represents the greatest value possible; that is, Mn^{2+} cannot stabilize an incorrect nucleotide in the 3D^{pol} active site better than a correct nucleotide. Our reasoning for this is as follows. Formation of the activated ternary complex occurs as a result of the normal dynamical motions of the enzyme and with a rate that is independent of the nature of the bound nucleotide. However, the rate of decay (i.e., stability) of this complex is dependent upon the nature of bound nucleotide (i.e., correct vs incorrect). A correct nucleotide should have more stable interactions in the activated ternary complex than an incorrect nucleotide. Consequently, the rate constant for opening from the closed conformation would be reduced for a correct nucleotide relative to an incorrect nucleotide. When Mn^{2+} is employed as the divalent cation, the conformation of the metal-B-bound triphosphate coupled with the additional adventitious interactions that can occur between the enzyme and Mn^{2+} increases the stability of this activated ternary complex; however, this increase in stability would be the same regardless of the configuration of the nucleotide, i.e., correct or incorrect. Therefore, we can assume that the value for $K_{2,2'\text{-dATP},Mg^{2+}}$ cannot exceed $K_{2,2'\text{-dATP},Mn^{2+}}/5$ (Table 4); the same logic applies to the calculation of the $K_{2,GTP,Mg^{2+}}$ value (Table 4). The required phosphorothioate data are shown in Table 2. The calculations yielded values of 21 and 3 s^{-1} for the phosphoryl-transfer step when 2′-dAMP or GMP is incorporated into sym/sub-U, respectively. These data permit us to conclude that, in the presence of Mg^{2+}, 3D^{pol} uses not only the conformational-change step for nucleotide selection but also the phosphoryl-transfer step. Therefore, the fidelity loss observed in the presence of Mn^{2+} results from the capacity of this divalent cation to disconnect the line of communication between the nucleoside-binding pocket and the catalytic center.

DISCUSSION

In this study, we elucidated the complete kinetic mechanism for 3D^{pol}-catalyzed nucleotide incorporation in the presence of Mn^{2+} in order to obtain greater insight into the molecular basis for the changes in catalytic efficiency, substrate selection, and incorporation fidelity observed by using this divalent cation cofactor instead of Mg^{2+} (7). Because Mn^{2+} changes the biochemical properties of essentially all nucleic acid polymerases, a mechanistic description of Mn^{2+}-induced effects in the context of the RdRP might also provide some insight into the mechanistic basis for Mn^{2+}-induced effects in other polymerase systems (4,5,7-10).

We found that the sequence of events employed by 3D^{pol} in the presence of Mn^{2+} for incorporation of a single, correct nucleotide was not different from that determined in the presence of Mg^{2+} (Scheme 1). We were able to obtain a single set of rate constants (Table 5) that were sufficient to model all of the experimental data (Figures 2, 3, 5, and 6). The experimental data provided good constraints on all of the rate constants preceding the second conformational-change step, suggesting no greater than a 2-fold error in any of these key parameters (Table 6).

NIH-PA Author Manuscript

NIH-PA Author Manuscript

NIH-PA Author Manuscript

In the presence of Mn^{2+}, the rate-limiting step for single nucleotide incorporation is the step attributed to phosphoryl transfer. This is an important observation because it permitted us to determine empirically the maximal value for the phosphorothioate effect with this polymerase. Knowledge of this value permits calculation of the values for K_2 or k_{+3} (eqs 3-5). In the past, there has been a controversy regarding the range for the phosphorothioate effect (20,21) and the utility of this parameter for defining rate-limiting steps in polymerase-catalyzed phosphoryl-transfer reactions (22). Our data suggest that, for polymerase-catalyzed phosphoryl-transfer reactions, the phosphorothioate effect may range from 8 to 11, consistent with data obtained by Herschlag, Piccirilli, and Cech for nonenzymatic phosphoryl-transfer reactions (20). We were able to exploit this information to provide all of the necessary values (Tables 1 and 4 and parameters reported in ref 12) to perform a thermodynamic comparison of $3D^{pol}$-catalyzed incorporation of a single correct or incorrect nucleotide in the presence of Mg^{2+} or Mn^{2+} (Figure 7). This analysis shows that $3D^{pol}$ can use all of the steps from ground-state binding of nucleotide to phosphoryl transfer for nucleotide selection; however, the extent to which each step is employed, if at all, is dependent upon the divalent cation cofactor.

Ground-state binding is not a significant factor for nucleotide selection in the presence of Mg^{2+} (Figure 7A), consistent with the possibility that this binding event is governed primarily by the triphosphate moiety of the bound nucleotide. In the presence of Mn^{2+}, ground-state binding of the correct nucleotide (ATP) is 2.4 kcal/mol more stable than in the presence of Mg^{2+}. This observation may suggest that Mn^{2+} has additional, adventitious interactions with the enzyme, for example, interactions with the backbone or nitrogen- or sulfur-containing residues located in or near the binding site for this metal. It is known that Mn^{2+}, being a transition metal, will interact with nitrogen and sulfur ligands better than Mg^{2+} (23). In the presence of Mn^{2+}, this step contributes 1.0-2.3 kcal/mol to the overall fidelity of nucleotide incorporation.

The conformational change preceding phosphoryl transfer is a step in the mechanism that is used by $3D^{pol}$ for nucleotide selection in a cation-independent manner. The free energy diagrams were constructed by assuming that k_{-2} is the mediator of fidelity at this stage of incorporation. Unfortunately, our experiments could not determine whether formation and/or stability of the “activated” ternary complex mediated selection. Additional studies will be required to clarify this issue. Interestingly, the overall contribution of the conformational-change step to nucleotide selection by $3D^{pol}$ is cation dependent. In the presence of Mn^{2+}, the conformational-change step represents the greatest contribution to the overall fidelity of $3D^{pol}$ (2.1-4.7 kcal/mol). However, in the presence of Mg^{2+}, the contribution of the conformational-change step to the overall fidelity is less (1.4-2.5 kcal/mol) and is shared with the subsequent step, phosphoryl transfer (2.0-3.0 kcal/mol). The phosphoryl-transfer step is not used at all for nucleotide selection in the presence of Mn^{2+}. The inability to couple the nature of the bound nucleotide to the efficiency of phosphoryl transfer is the primary reason for the observed loss of $3D^{pol}$ fidelity in the presence of Mn^{2+}.

Our current model to explain the cation-dependent nucleotide-selection process of $3D^{pol}$ is illustrated in Figure 8. Binding of Mg^{2+}/Mn^{2+}-NTP to the $3D^{pol}$-primer/template complex is driven by the metal-complexed triphosphate moiety of the nucleotide (Figure 8A). The increased affinity of Mn^{2+}-NTP may reflect the presence of adventitious interactions in the pocket. The greatest number of interactions will occur with the correct nucleotide, permitting this step to provide some discrimination between correct nucleotides and nucleotides containing an incorrect sugar configuration or base (Figure 7B).

Once Mg^{2+}/Mn^{2+}-NTP is bound, a conformational change of the metal-complexed triphosphate moiety brings this metal into the appropriate position to interact with the conserved aspartyl groups of the enzyme and, at the same time, organizes the active site for

NIH-PA Author Manuscript

NIH-PA Author Manuscript

NIH-PA Author Manuscript

acceptance of the second metal ion required for catalysis (Figure 8B). Again, the enhancement of the stability of this complex in the presence of Mn^{2+} could reflect additional, unique interactions. However, in this complex, these extra interactions may effectively overcompensate for those interactions used to stabilize this complex when Mg^{2+} is employed as the divalent cation cofactor. If, in the presence of Mg^{2+}, the interactions with the actively oriented triphosphate originate from the ribose-binding pocket, then the presence of an incorrect sugar configuration or an incorrect base could alter these interactions, simultaneously changing K_2 and k_{+3}. The change in k_{+3} would be caused by the inability to maintain the triphosphate in the catalytically competent conformation. In the presence of Mn^{2+}, however, disruption of the interactions between the triphosphate of an incorrect nucleotide and residues in the ribose-binding pocket would be compensated for by the additional Mn^{2+}-specific interactions, thereby preventing a reduction in the value for k_{+3}.

Once reorientation of the triphosphate moiety occurs, the second metal will bind (Figure 8C) and catalysis will occur (Figure 8D). While Mg^{2+} is perfectly suited to this pocket, the subtle increase in the ionic radius of Mn^{2+} (0.75 Å) relative to Mg^{2+} (0.65 Å) may be sufficient to alter the distance between the primer 3′-OH and the α-phosphorus of the nucleotide substrate, causing the observed 17-fold reduction in the rate of phosphoryl transfer. Indeed, Carey and colleagues have shown that a 0.015 Å change in bond length can cause a 500-fold change in reactivity of serine protease substrates (24, 25). Additional studies will be required to determine whether binding of the second metal, deprotonation of the 3′-OH, or some other step is actually limiting the rate of phosphoryl transfer in the presence of Mn^{2+}.

A distinguishing feature of this mechanism is the interpretation that the conformational change preceding catalysis is reorientation of the metal-complexed triphosphate moiety of the nucleotide from its ground-state configuration (Figure 8A) to the catalytically competent configuration (Figure 8B). All of the data reported herein demonstrate that the conformational change is the metal-sensitive step. Because the triphosphate portion of the nucleotide substrate has a large set of interactions with the metals, it is reasonable to conclude that the triphosphate is involved somehow in the conformational change. This interpretation is supported by the recent work of Beese and co-workers that has provided detailed structural evidence for reorientation of the triphosphate moiety of the nucleotide substrate during successive cycles of nucleotide incorporation catalyzed by the large fragment of DNA polymerase I from *Bacillus stearothermophilus* (BF) (26). In addition, this hypothesis was put forward by Mildvan and colleagues (27, 28) and Benkovic and colleagues (15) in their studies of the Klenow fragment of DNA polymerase I from *Escherichia coli*. The current view that the conformational change observed kinetically reflects rigid-body movements of the polymerase fingers subdomain has never been proved, and recent data from the Wilson and Beese laboratories refute this possibility convincingly (26, 29). Because the mechanistic studies of $3D^{pol}$-catalyzed nucleotide incorporation (12) provide a better mechanistic connection to the Klenow fragment of DNA polymerase I (15) than to any other systems for which detailed kinetic and structural studies are available (13, 15, 17, 26, 30-38), the structural studies of BF provide the best structural surrogate for $3D^{pol}$.

All polymerases reported to date exhibit the greatest fidelity in the presence of Mg^{2+} (2), and most structural studies provide evidence for the formation of extensive interactions between the enzyme and nucleotide substrate in complexes poised for or undergoing catalysis (1,26, 30,33,39). Many of these interactions are in a position in which inappropriate sugar configurations or base pairing would perturb these interactions, producing the same deleterious effects on the equilibrium position of the isomerized ternary complex and phosphoryl transfer as observed for $3D^{pol}$. In these systems, Mn^{2+} may also be able to suppress and/or compensate for distortions caused by the binding of incorrect nucleotides or the presence of modified template bases, again through adventitious interactions of the Mn^{2+} cofactor with the enzyme.

NIH-PA Author Manuscript

NIH-PA Author Manuscript

NIH-PA Author Manuscript

Consistent with this possibility is the finding by the Berdis laboratory that the major defect for T4 DNA polymerase-catalyzed incorporation of nucleotides opposite an abasic site in DNA is a reduction in K_2 that can be overcome by using Mn^{2+} instead of Mg^{2+} as the cofactor (40).

Given the capacity of the metal employed in polymerase-catalyzed reactions to have an effect not only on substrate selection and incorporation fidelity but also on rate-limiting steps during the nucleotide incorporation cycle, some caution is warranted when studies employing alternative metal cofactors are used to reach general conclusions regarding the polymerase mechanism.

CONCLUSION

This report combined with the preceding paper (12) provides the first comprehensive quantitative evaluation of RNA-dependent RNA polymerase-catalyzed nucleotide incorporation. This class of enzymes employs the same overall mechanism for nucleotide incorporation and fidelity as the other classes of nucleic acid polymerases. Both the conformational change preceding phosphoryl transfer and phosphoryl transfer are partially rate limiting for nucleotide incorporation in the presence of Mg^{2+}, and both of these steps are employed for nucleotide selection and incorporation fidelity in the presence of this divalent cation cofactor. In contrast, in the presence of Mn^{2+}, the ability to use the phosphoryl-transfer step for incorporation fidelity is lost, leaving primarily the conformational-change step to accomplish this important task. With this kinetic framework in hand, elucidation of the structural features of the enzyme that dictate the observed kinetic pathway should be possible. Unique structural features of the RNA-dependent RNA polymerase essential for enzyme function should prove to be important targets for the design of agents to selectively inhibit the RNA-dependent RNA polymerase without affecting the myriad cellular polymerases required for life.

ACKNOWLEDGMENT

We thank Professor J. Martin Bollinger for very insightful, enthusiastic discussions. We also thank Professor Kevin D. Raney for critical review of the manuscript.

REFERENCES

1. Brautigam CA, Steitz TA. Structural and functional insights provided by crystal structures of DNA polymerases and their substrate complexes. Curr. Opin. Struct. Biol 1998;8:54–63. [PubMed: 9519297]
2. Kornberg, A.; Baker, T. DNA Replication. 2nd ed.. W. H. Freeman and Co.; New York: 1991.
3. Grabbara S, Peliska JA. Catalytic activities associated with retroviral and viral polymerases. Methods Enzymol 1996;275:276–310. [PubMed: 9026644]
4. Tabor S, Richardson CC. Effect of manganese ions on the incorporation of dideoxynucleotides by bacteriophage T7 DNA polymerase and *Escherichia coli* DNA polymerase I. Proc. Natl. Acad. Sci. U.S.A 1989;86:4076–4080. [PubMed: 2657738]
5. Huang Y, Beaudry A, McSwiggen J, Sousa R. Determinants of ribose specificity in RNA polymerization: effects of Mn^{2+} and deoxynucleoside monophosphate incorporation into transcripts. Biochemistry 1997;36:13718–13728. [PubMed: 9354643]
6. Brooks RR, Anderson JA. Substrate, metal and template effects on inhibition of bacteriophage-qbeta ribonucleic acid polymerase by ortho- and pyro-phosphate. Biochem. J 1978;171:725–732. [PubMed: 208514]
7. Arnold JJ, Ghosh SK, Cameron CE. Poliovirus RNA-dependent RNA polymerase ($3D^{pol}$): Divalent cation modulation of primer, template, and nucleotide selection. J. Biol. Chem 1999;274:37060–37069. [PubMed: 10601264]
8. Beckman RA, Mildvan AS, Loeb LA. On the fidelity of DNA replication: manganese mutagenesis in vitro. Biochemistry 1985;24:5810–5817. [PubMed: 3910084]

NIH-PA Author Manuscript

NIH-PA Author Manuscript

NIH-PA Author Manuscript

9. Liu J, Tsai M-D. DNA polymerase beta: Pre-steady-state kinetic analyses of dATPalphaS stereoselectivity and alteration of the stereoselectivity by various metal ions and by site-directed mutagenesis. Biochemistry 2001;40:9014–9022. [PubMed: 11467964]
10. Goodman MF, Keener S, Guidotti S, Branscomb EW. On the enzymatic basis for mutagenesis by manganese. J. Biol. Chem 1983;258:3469–3475. [PubMed: 6833210]
11. Arnold JJ, Cameron CE. Poliovirus RNA-dependent RNA polymerase ($3D^{pol}$): Assembly of stable, elongation-competent complexes by using a symmetrical primer-template substrate (sym/sub). J. Biol. Chem 2000;275:5329–5336. [PubMed: 10681506]
12. Arnold JJ, Cameron CE. Poliovirus RNA-dependent RNA polymerase ($3D^{pol}$): Pre-steady-state kinetic analysis of ribonucleotide incorporation in the presence of Mg^{2+} Biochemistry 2004;43:5126–5137. [PubMed: 15122878]
13. Kati WM, Johnson KA, Jerva LF, Anderson KS. Mechanism and fidelity of HIV reverse transcriptase. J. Biol. Chem 1992;267:25988–25997. [PubMed: 1281479]
14. Hsieh JC, Zinnen S, Modrich P. Kinetic mechanism of the DNA-dependent DNA polymerase activity of human immunodeficiency virus reverse transcriptase. J. Biol. Chem 1993;268:24607–24613. [PubMed: 7693703]
15. Kuchta RD, Mizrahi V, Benkovic PA, Johnson KA, Benkovic SJ. Kinetic mechanism of DNA polymerase I (Klenow). Biochemistry 1987;26:8410–8417. [PubMed: 3327522]
16. Dahlberg ME, Benkovic SJ. Kinetic mechanism of DNA polymerase I (Klenow Fragment): Identification of a second conformational change and evaluation of the internal equilibrium constant. Biochemistry 1991;30:4835–4845. [PubMed: 1645180]
17. Patel SS, Wong I, Johnson KA. Pre-steady-state kinetic analysis of processive DNA replication including complete characterization of an exonuclease-deficient mutant. Biochemistry 1991;30:511–525. [PubMed: 1846298]
18. Gohara DW, Crotty S, Arnold JJ, Yoder JD, Andino R, Cameron CE. Poliovirus RNA-dependent RNA polymerase ($3D^{pol}$): Structural, biochemical, and biological analysis of conserved structural motifs A and B. J. Biol. Chem 2000;275:25523–25532. [PubMed: 10827187]
19. Gohara DW, Ha CS, Kumar S, Ghosh B, Arnold JJ, Wisniewski TJ, Cameron CE. Production of "authentic" poliovirus RNA-dependent RNA polymerase ($3D^{pol}$) by ubiquitin-protease-mediated cleavage in *Escherichia coli*. Protein Expression Purif 1999;17:128–138.
20. Herschlag D, Piccirilli JA, Cech TA. Ribozyme-catalyzed and nonenzymatic reactions of phosphate diesters: Rate effects upon substitution of sulfur for a nonbridging phosphoryl oxygen atom. Biochemistry 1991;30:4844–4854. [PubMed: 2036355]
21. Benkovic, SJ.; Schray, KJ. The Enzymes. 3rd ed.. Academic Press; New York: 1971.
22. Showalter AK, Tsai M-D. A reexamination of the nucleotide incorporation fidelity of DNA polymerases. Biochemistry 2002;41:10571–10576. [PubMed: 12186540]
23. Bock CW, Katz AK, Markham GD, Glusker JP. Manganese as a replacement for magnesium and zinc: functional comparison of the divalent ions. J. Am. Chem. Soc 1999;121:7360–7372.
24. Tonge PJ, Carey PR. Length of the acyl carbonyl bond in acyl-serine proteases correlates with reactivity. Biochemistry 1990;29:10723–10727. [PubMed: 2271679]
25. Tonge PJ, Carey PR. Forces, bond lengths, and reactivity: fundamental insight into the mechansim of enzyme catalysis. Biochemistry 1992;31:9122–9125. [PubMed: 1390699]
26. Johnson SJ, Taylor JS, Beese LS. Processive DNA synthesis observed in a polymerase crystal suggests a mechanism for the prevention of frameshift mutations. Proc. Natl. Acad. Sci. U.S.A 2003;100:3985–3900.
27. Ferrin LJ, Mildvan AS. Nuclear overhauser effect studies of the conformations and binding site environments of deoxynucleoside triphosphate substrates bound to DNA polymerse I and Its large fragment. Biochemistry 1985;24:6904–6912. [PubMed: 3907705]
28. Ferrin LJ, Mildvan AS. Studies of conformations and interactions of substrates and ribonucleotide templates bound to the large fragment of DNA polymerase I. Biochemistry 1986;25:5131–5145. [PubMed: 3533145]
29. Van de Berg BJ, Beard WA, Wilson SH. DNA structure and aspartate 276 influence nucleotide binding to human DNA polymerase beta. Implication for the identity of the rate-limiting conformational change. J. Biol. Chem 2001;276:3408–3416. [PubMed: 11024043]

NIH-PA Author Manuscript

NIH-PA Author Manuscript

NIH-PA Author Manuscript

30. Doublie S, Tabor S, Long AM, Richardson CC, Ellenberger T. Crystal structure of a bacteriophage T7 DNA replication complex at 2.2 A resolution. Nature 1998;391:251–258. [PubMed: 9440688]

31. Beese LS, Friedman JM, Steitz TA. Crystal structures of the Klenow fragment of DNA polymerase I complexed with deoxynucleoside triphosphate and pyrophosphate. Biochemistry 1993;32:14095–14101. [PubMed: 8260491]

32. Freemont PS, Friedman JM, Beese LS, Sanderson MR, Steitz TA. Cocrystal structure of an editing complex of Klenow fragment with DNA. Proc. Natl. Acad. Sci. U.S.A 1988;85:8924–8928. [PubMed: 3194400]

33. Huang H, Chopra R, Verdine GL, Harrison SC. Structure of a covalently trapped catalytic complex of HIV-1 reverse transcriptase: implications for drug resistance. Science 1998;282:1669–1675. [PubMed: 9831551]

34. Rodgers DW, Gamblin SJ, Harris BA, Ray S, Culp JS, Hellmig B, Woolf DJ, Debouck C, Harrison SC. The structure of unliganded reverse transcriptase from the human immunodeficiency virus type 1. Proc. Natl. Acad. Sci. U.S.A 1995;92:1222–1226. [PubMed: 7532306]

35. Arndt JW, Weimin G, Zhong X, Showalter AK, Liu J, Dunlap CA, Lin Z, Paxson C, Tsai M-D, Chan MK. Insight into the catalytic mechanism of DNA polymerase beta: Structures of intermediate complexes. Biochemistry 2001;40:5368–5375. [PubMed: 11330999]

36. Dunlap CA, Tsai M-D. Use of 2-aminopurine and tryptophan fluorescence as probes in kinetic analyses of DNA polymerase beta. Biochemistry 2002;41:11226–11235. [PubMed: 12220188]

37. Pelletier H, Sawaya MR, Wolfle W, Wilson SH, Kraut J. Crystal structures of human DNA polymerase beta complexed with DNA: Implications for catalytic mechanism, processivity, and fidelity. Biochemistry 1996;35:12742–12761. [PubMed: 8841118]

38. Pelletier H, Sawaya MR, Wolfle W, Wilson SH, Kraut J. A structural basis for metal ion mutagenicity and nucleotide selectivity in human DNA polymerase beta. Biochemistry 1996;35:12762–12777. [PubMed: 8841119]

39. Kiefer JR, Mao C, Braman JC, Beese LS. Visualizing DNA replication in a catalytically active Bacillus DNA polymerase crystal. Nature 1998;391:304–307. [PubMed: 9440698]

40. Hays H, Berdis AJ. Manganese substantially alters the dynamics of translesion DNA synthesis. Biochemistry 2002;41:4771–4778. [PubMed: 11939771]

41. Wong I, Patel SS, Johnson KA. An induced-fit kinetic mechanism for DNA replication fidelity: direct measurement by single-turnover kinetics. Biochemistry 1991;30:526–537. [PubMed: 1846299]

NIH-PA Author Manuscript

NIH-PA Author Manuscript

NIH-PA Author Manuscript

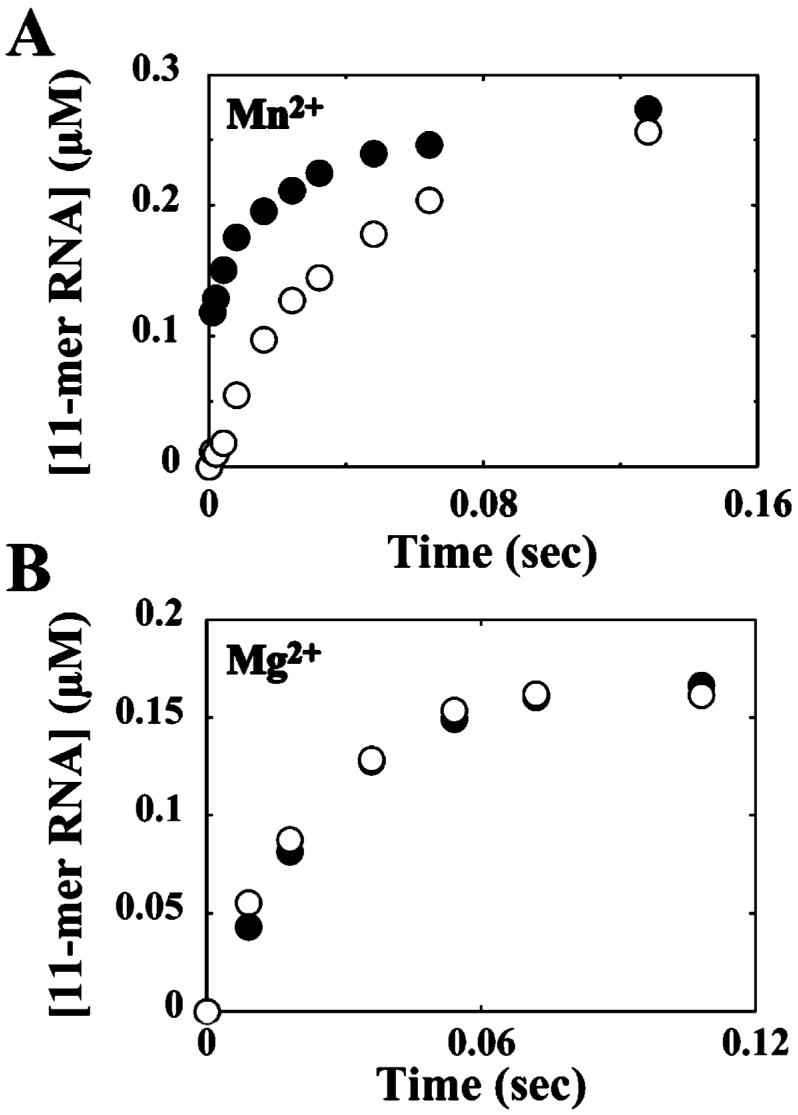

FIGURE 1.

The observed kinetics of $3D^{pol}$-catalyzed nucleotide incorporation in the presence of Mn^{2+} is dependent upon the nature of the quench. (A) Kinetics of AMP incorporation in the presence of Mn^{2+} quenched by either EDTA (●) or HCl (○). 2 μM $3D^{pol}$ was incubated with 2 μM sym/sub (1 μM duplex) and rapidly mixed with 500 μM ATP (final concentration) in the presence of Mn^{2+} as described under Experimental Procedures. (B) Kinetics of AMP incorporation in the presence of Mg^{2+} quenched by either EDTA (●) or HCl (○). 2 μM $3D^{pol}$ was incubated with 2 μM sym/sub (1 μM duplex) and rapidly mixed with 500 μM ATP (final concentration) in the presence of Mg^{2+} as described under Experimental Procedures.

NIH-PA Author Manuscript

NIH-PA Author Manuscript

NIH-PA Author Manuscript

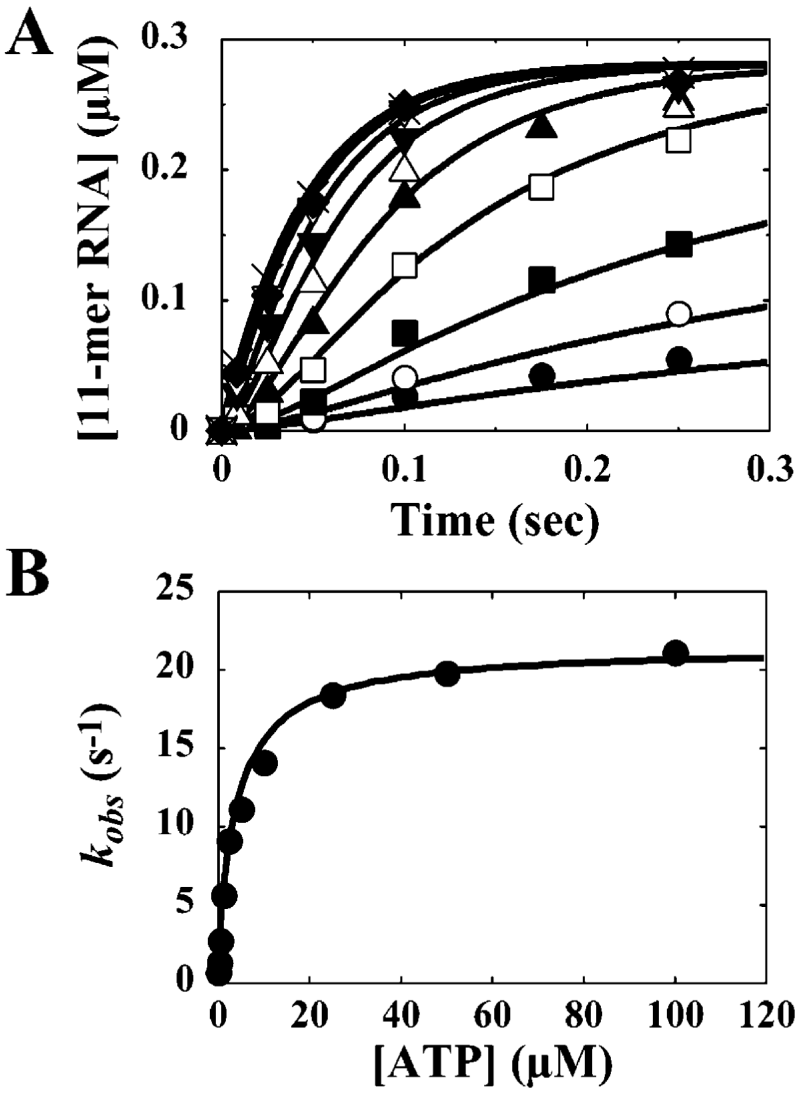

FIGURE 2.

Concentration dependence of AMP incorporation into sym/sub. 2 μM $3D^{pol}$ was incubated with 2 μM sym/sub (1 μM duplex) and rapidly mixed with either 0.125 (●), 0.25 (○), 0.5 (■), 1.25 (□), 2.5 (▲), 5 (△), 10 (▼), 20 (▽), 50 (◆), or 100 (×) μM (final concentration) ATP as described under Experimental Procedures. The solid lines represent the kinetic simulation of the mechanism shown in Scheme 1 with the kinetic parameters shown in Table 5. (B) k_{obs} as a function of ATP concentration obtained from the reactions described in (A). The solid line represents the fit of the data to a hyperbola with a $K_{d,app}$ for ATP of 4.1 ± 0.5 μM and a k_{pol} of 21.4 ± 0.6 s^{-1}.

NIH-PA Author Manuscript

NIH-PA Author Manuscript

NIH-PA Author Manuscript

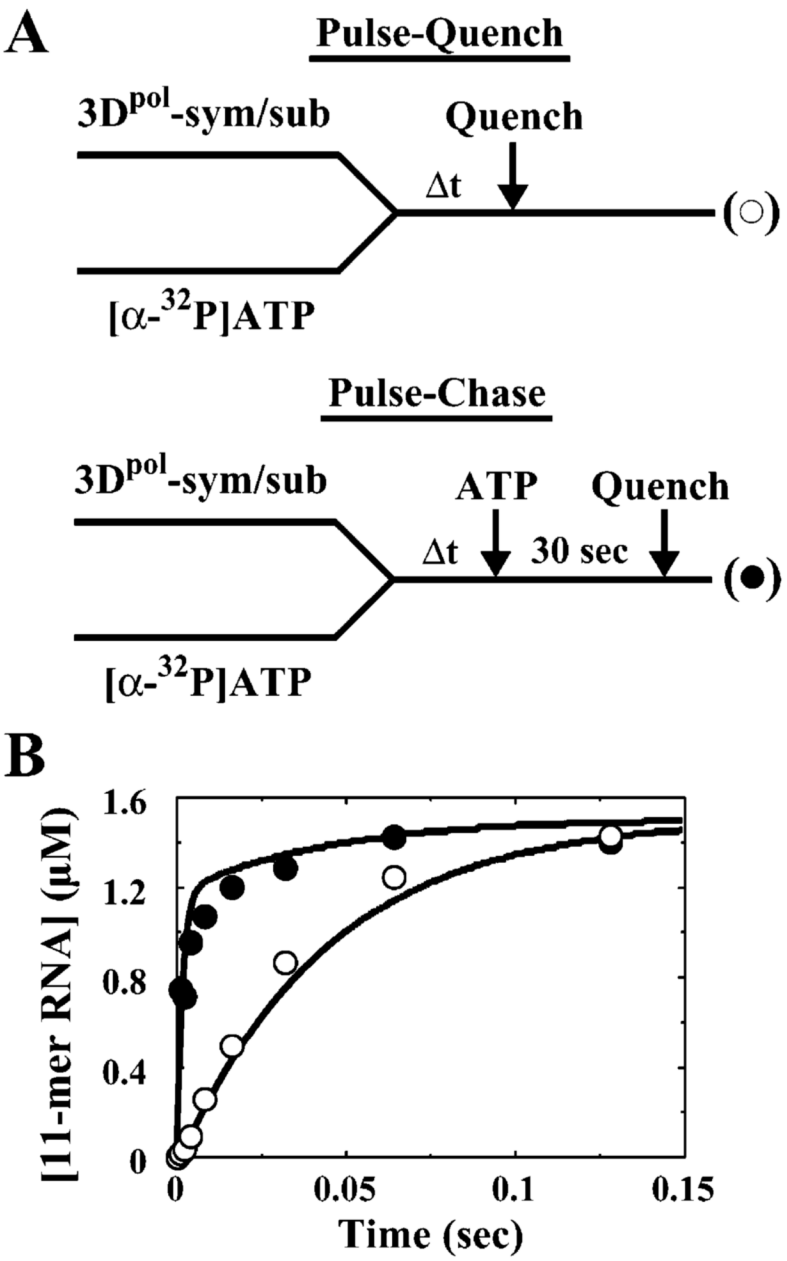

FIGURE 3.

Intermediate identification by pulse-chase analysis. (A) Experimental design. 4 μM 3D^{pol} was incubated with 20 μM sym/sub (10 μM duplex) and rapidly mixed with 130 μM [α-^{32}P]ATP (3.8 Ci/mmol) (final concentration) as described under Experimental Procedures. At the indicated times, reactions were either chased by addition of ATP to a final concentration of 20 mM or quenched by addition of HCl to a final concentration of 1 M. After addition of the chase solution, the reaction was allowed to proceed for an additional 30 s, at which time the reaction was quenched by addition of HCl to a final concentration of 1 M. Immediately after addition of HCl, the solution was neutralized by addition of 1 M KOH and 300 mM Tris. (B) Kinetics of pulse-chase (●) and pulse-quench (○) from the reactions described in (A). The solid lines represent the kinetic simulation of the data fit to the mechanism shown in Scheme 1 with the kinetic parameters shown in Table 5. The simulated curve of the pulse-quench data predicts

the rate of formation of all R_{n+1}-containing species; the simulated curve of the pulse-chase data predicts the rate of formation of *ER_nNTP and all R_{n+1}-containing species.

NIH-PA Author Manuscript
NIH-PA Author Manuscript
NIH-PA Author Manuscript

NIH-PA Author Manuscript

NIH-PA Author Manuscript

NIH-PA Author Manuscript

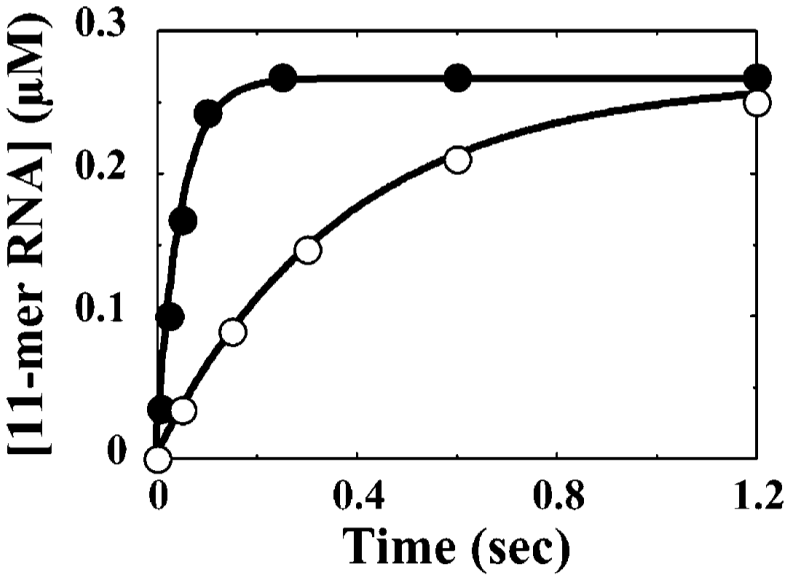

FIGURE 4.

Elemental effect on the pre-steady-state burst rate of AMP incorporation. (A) 2 μM 3D^{pol} was incubated with 2 μM sym/sub (1 μM duplex) and rapidly mixed with either 100 μM ATP (●) or 100 μM ATPαS (○) (final concentration) as described under Experimental Procedures. The solid lines represent the fit of the data to a single exponential with a k_{obs} for ATP of 20.4 ± 0.8 s^{-1} and a k_{obs} for ATPαS of 2.67 ± 0.04 s^{-1}.

NIH-PA Author Manuscript

NIH-PA Author Manuscript

NIH-PA Author Manuscript

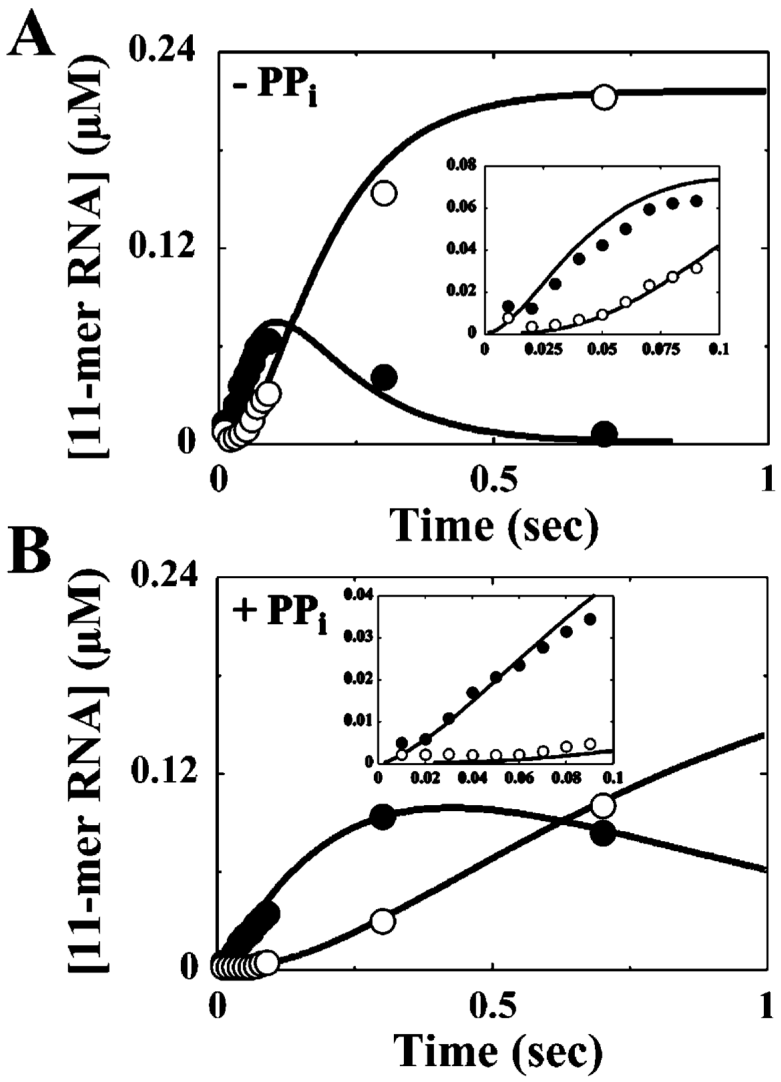

FIGURE 5.

Multiple nucleotide incorporation in the absence and presence of pyrophosphate. (A) 2 μM $3D^{pol}$ was incubated with 2 μM sym/sub (1 μM duplex) and rapidly mixed with 4 μM ATP and 7 μM UTP (final concentration) as described under Experimental Procedures. Key: Kinetics of formation and disappearance of 11-mer (●) and 12-mer (○). The solid lines represent the kinetic simulation of the data fit to a mechanism for two successive nucleotide incorporations with the first nucleotide incorporation described by the kinetic mechanism shown in Scheme 1 using the kinetic parameters in Table 5 and the second nucleotide incorporation described by the mechanism shown in Scheme 4 using the $K_{d,app}$ and k_{pol} values for UTP using sym/sub-UA shown in Table 1. (B) 2 μM $3D^{pol}$ was incubated with 2 μM sym/sub (1 μM duplex) and rapidly mixed with 4 μM ATP, 7 μM UTP, and 1000 μM PP_i (final concentration) as described under Experimental Procedures. Key: Kinetics of formation and disappearance of 11-mer (●) and 12-mer (○). The solid lines represent the kinetic simulation of the data fit to a mechanism for two successive nucleotide incorporations with the first nucleotide incorporation described by the kinetic mechanism shown in Scheme 1 using the kinetic parameters in Table 5 and the second nucleotide incorporation described by the mechanism shown in Scheme 4 using the $K_{d,app}$ and k_{pol} values for UTP using sym/sub-UA shown in Table 1.

NIH-PA Author Manuscript

NIH-PA Author Manuscript

NIH-PA Author Manuscript

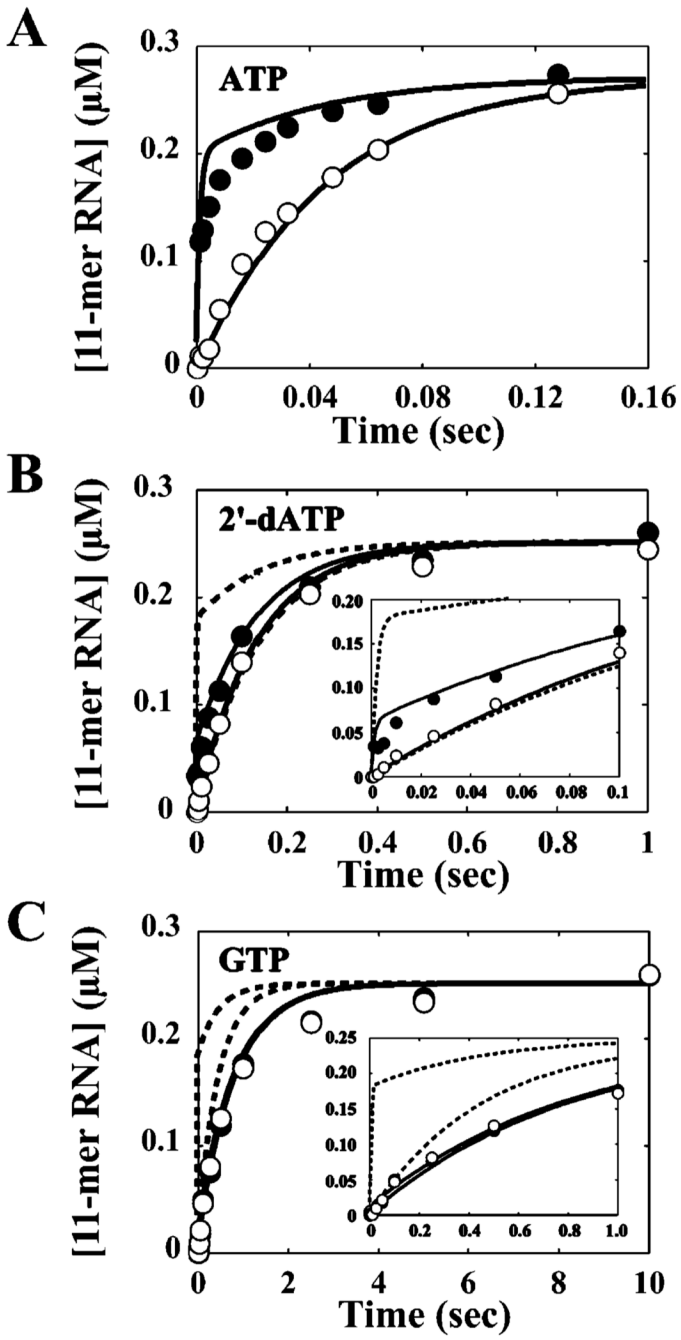

FIGURE 6.

The amount of intermediate that accumulates prior to chemistry for incorrect nucleotide incorporation is reduced relative to correct incorporation. (A) Kinetics of AMP incorporation in the presence of Mn^{2+} quenched by either EDTA (●) or HCl (○). The solid line represents the kinetic simulation of the data fit to the mechanism shown in Scheme 2 with K_2 equal to 3 and k_{+3} equal to 30 s^{-1}. 2 μM $3D^{pol}$ was incubated with 2 μM sym/sub (1 μM duplex) and rapidly mixed with 500 μM ATP (final concentration) as described under Experimental Procedures. (B) Kinetics of 2′-dAMP incorporation in the presence of Mn^{2+} quenched by either EDTA (●) or HCl (○). The solid line represents the kinetic simulation of the data fit to the mechanism shown in Scheme 2 with K_2 equal to 0.4 and k_{+3} equal to 30 s^{-1}. The dotted line

NIH-PA Author Manuscript

NIH-PA Author Manuscript

NIH-PA Author Manuscript

represents the kinetic simulation of the data fit to the mechanism shown in Scheme 2 with K_2 equal to 3 and k_{+3} equal to 10 s^{-1}. 2 μM $3D^{pol}$ was incubated with 2 μM sym/sub (1 μM duplex) and rapidly mixed with 500 μM 2′-dATP (final concentration) as described under Experimental Procedures. (C) Kinetics of GMP incorporation in the presence of Mn^{2+} quenched by either EDTA (●) or HCl (○). The solid line represents the kinetic simulation of the data fit to the mechanism shown in Scheme 2 with K_2 equal to 0.05 and k_{+3} equal to 30 s^{-1}. The dotted line represents the kinetic simulation of the data fit to the mechanism shown in Scheme 2 with K_2 equal to 3 and k_{+3} equal to 3 s^{-1}. 2 μM $3D^{pol}$ was incubated with 2 μM sym/sub (1 μM duplex) and rapidly mixed with 1000 μM GTP (final concentration) as described under Experimental Procedures.

NIH-PA Author Manuscript
NIH-PA Author Manuscript
NIH-PA Author Manuscript

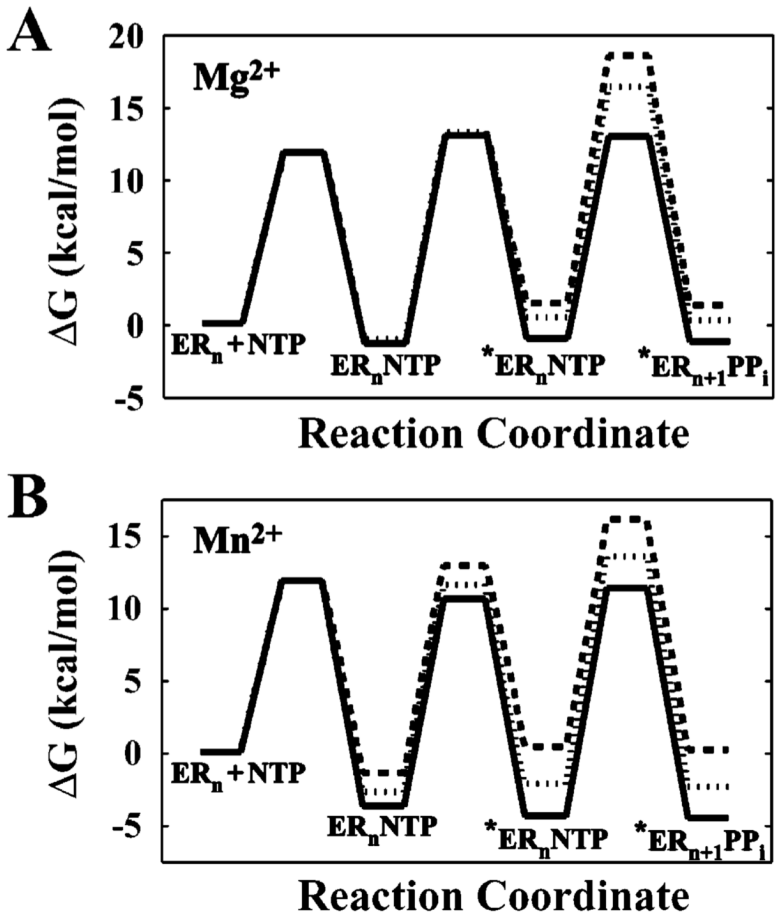

FIGURE 7.

Comparison of the free energy profile for correct and incorrect $3D^{pol}$-catalyzed nucleotide incorporation in the presence of Mg^{2+} and Mn^{2+}. (A) Free energy profile in the presence of Mg^{2+}. The free energy profile for correct and incorrect nucleotide incorporation is shown as follows: solid line for AMP incorporation, small dotted line for 2′-dAMP incorporation, and large dotted line for GMP incorporation. (B) Free energy profile in the presence of Mn^{2+}. The free energy profile for correct and incorrect nucleotide incorporation is shown as follows: solid line for AMP incorporation, small dotted line for 2′-dAMP incorporation, and large dotted line for GMP incorporation. The concentrations of the substrates and products used were 2000 μM NTP and 20 μM PP_i. The free energy for each reaction step was calculated from $\Delta G = RT[\ln(-(kT/h) - \ln(k_{obs})]$, where R is 1.99 cal K^{-1} mol^{-1}, T is 303 K, k is 3.30×10^{-24} cal K^{-1}, h is 1.58×10^{-34} cal s, and k_{obs} is the first-order rate constant. The free energy for each species was calculated from $\Delta G = RT[\ln(kT/h) - \ln(k_{obs,for})] - RT[\ln(kT/h) - \ln(k_{obs,rev})]$.

NIH-PA Author Manuscript

NIH-PA Author Manuscript

NIH-PA Author Manuscript

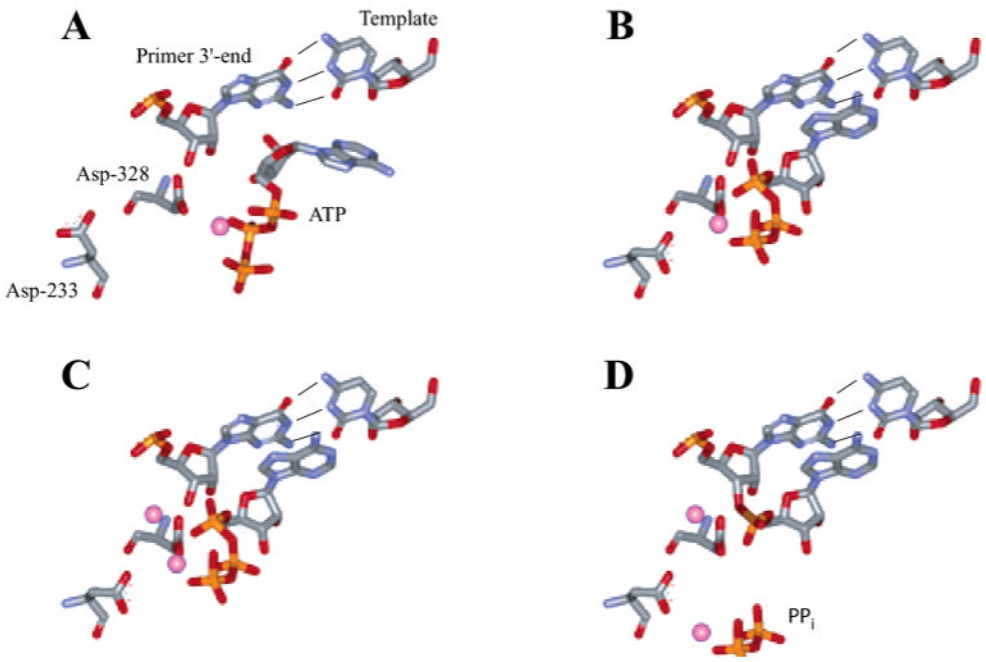

FIGURE 8.

Structural model for $3D^{pol}$-catalyzed nucleotide incorporation. (A) Ground-state binding of metal-complexed nucleotide. (B) Reorientation of the triphosphate into the catalytically competent configuration. (C) Binding of the second metal ion. (D) Phosphoryl transfer and pyrophosphate release. While the kinetic mechanism suggests a conformational change prior to pyrophosphate release, our data do not provide any information to permit a molecular description of this step. Images were generated from the model previously described (18). Nucleotide and side chain motions were derived from ref 26 by approximate rotation and translation movements. Atom colors correspond to the following: red, oxygen; blue, nitrogen; gray, carbon; magenta, Mg^{2+} or Mn^{2+}. The images were rendered with WebLab Viewer Pro (Accelrys Inc., San Diego, CA).

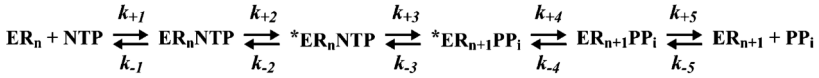

Scheme 1.

Complete Kinetic Mechanism for $3D^{pol}$-Catalyzed Nucleotide Incorporation[a]

[a] Abbreviations: ER_n, $3D^{pol}$-sym/sub complex; NTP, nucleotide; ER_nNTP, ternary complex; $*ER_nNTP$, activated elongation complex; $*ER_{n+1}PP_i$, activated product complex; $ER_{n+1}PP_i$, product complex; ER_{n+1}, $3D^{pol}$ sym/sub product complex; PP_i, pyrophosphate.

NIH-PA Author Manuscript NIH-PA Author Manuscript NIH-PA Author Manuscript

NIH-PA Author Manuscript

NIH-PA Author Manuscript

NIH-PA Author Manuscript

Scheme 2.

Minimal Mechanism for Pulse-Chase Analysis[a]

[a] Abbreviations: ER_nNTP, ternary complex; $^*ER_nNTP$, activated elongation complex; ER_n+1PP_i, product complex.

NIH-PA Author Manuscript

NIH-PA Author Manuscript

NIH-PA Author Manuscript

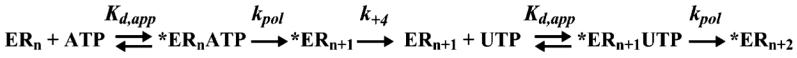

Scheme 3.

Minimal Kinetic Mechanism for Consecutive Incorporation of Two Nucleotides by $3D^{pol}$ [a]

[a] Abbreviations: ER_n, $3D^{pol}$-sym/sub complex; ATP, adenosine 5′-triphosphate; $*ER_nATP$, activated elongation complex; $*ER_{n+1}$, activated product complex 1; ER_{n+1}, product complex; UTP, uridine 5′-triphosphate; $*ER_{n+1}UTP$, activated elongation product complex 1; $*ER_{n+2}$, activated product complex 2.

NIH-PA Author Manuscript

NIH-PA Author Manuscript

NIH-PA Author Manuscript

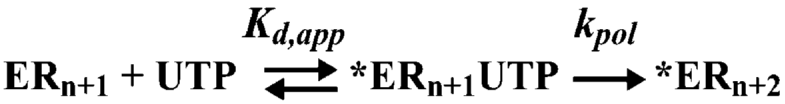

Scheme 4.

Minimal Kinetic Mechanism for UMP Incorporation into sym/sub-UA by $3D^{pol}$ [a]

[a] Abbreviations: ER_{n+1}, product complex; UTP, uridine 5′-triphosphate; $^*ER_{n+1}UTP$, activated elongation product complex 1; $^*ER_{n+2}$, activated product complex 2.

NIH-PA Author Manuscript

NIH-PA Author Manuscript

NIH-PA Author Manuscript

Table 1

Kinetic Constants for $3D^{pol}$-Catalyzed Nucleotide Incorporation in the Presence of Mn^{2+} [a]

substrates		kinetic parameters	
nucleic acid	**nucleotide**	$K_{d,app}$ (μM)	k_{pol} (s^{-1})
sym/sub-U			
GCA**U**GGGCCC CCCGGG**U**ACG	ATP	4.1 ± 0.5	21.4 ± 0.6
	ATPαS	1.0 ± 0.2	2.7 ± 0.1
	2′-dATP	19.2 ± 4.0	8.5 ± 0.6
	2′-dATPαS	11.3 ± 2.2	0.76 ± 0.04
	GTP	173 ± 20	1.7 ± 0.1
	GTP[b]	ND[c]	2.9 ± 0.3
	GTPαS[b]	ND[c]	0.51 ± 0.06
sym/sub-C			
GAU**C**GGGCCC CCCGGG**C**UAG	GTP[b]	ND[c]	35.3 ± 2.2
	GTPαS[b]	ND[c]	4.3 ± 0.2
sym/sub-UA			
GC**A**UGGGCCCA ACCCGGGU**A**CG	UTP	30.9 ± 3.9	86.8 ± 5.5

[a] Experiments were performed as described in the legend to Figure 1.

[b] The observed rate constant for nucleotide incorporation was determined at a concentration of 1 mM $MnCl_2$ and nucleotide concentrations of 50 and 500 μM. The difference between the rates at 50 and 500 μM was less than 5%.

[c] Not determined.

NIH-PA Author Manuscript

NIH-PA Author Manuscript

NIH-PA Author Manuscript

Table 2

Observed Phosphorothioate Effect for Correct and Incorrect Nucleotide Incorporation in the Presence of Mg^{2+} and Mn^{2+} [a]

nucleotide	Mg^{2+}	Mn^{2+}
correct		
ATP	4.2 ± 0.4	7.9 ± 0.4
GTP	ND[b]	8.2 ± 0.6
incorrect		
2′-dATP	6.2 ± 0.7	11 ± 1
GTP	2.4 ± 0.3	5.7 ± 0.9

[a] The observed phosphorothioate effect is calculated using $(k_{pol})_{NTP}/(k_{pol})_{NTP\alpha S}$. Values for k_{pol} are listed in Table 1.

[b] Not determined.

NIH-PA Author Manuscript

NIH-PA Author Manuscript

NIH-PA Author Manuscript

Table 3

Fidelity of 3D^{pol}-Catalyzed Nucleotide Incorporation in the Presence of Mg^{2+} and Mn^{2+}

	fidelity[a]		
nucleotide	**Mg^{2+}**	**Mn^{2+}**	**Mg^{2+}/Mn^{2+}**
2′-dATP	233	13	18
GTP	15477	532	29

[a] Fidelity is calculated as $[(k_{pol}/K_{d,app})ATP + (k_{pol}/K_{d,app})incorrect]/[(k_{pol}/K_{d,app})incorrect]$ (41). sym/sub-U was employed; therefore, ATP is the correct nucleotide. The values for $k_{pol}/K_{d,app}$ in the presence of Mg^{2+} were obtained from ref 12, and those in the presence of Mn^{2+} were obtained from Table 1.

NIH-PA Author Manuscript

NIH-PA Author Manuscript

NIH-PA Author Manuscript

Table 4

Comparison of K_2 and k_{+3} Values for Correct and Incorrect Nucleotide Incorporation in the Presence of Mg^{2+} and Mn^{2+}

	K_2		k_{+3} (s^{-1})	
nucleotide	**Mn^{2+}[a]**	**Mg^{2+}[b]**	**Mn^{2+}**	**Mg^{2+}[c]**
ATP	3	0.6	30	520
2′-dATP	0.4	0.08	30	21
GTP	0.05	0.01	30	3

[a] K_2 was determined by kinetic simulation of the data in Figure 6 fit to the mechanism shown in Scheme 2 with k_{+3} equal to 30 s^{-1}.

[b] K_2 for ATP was taken from ref 12, and the values for 2′-dATP and GTP were calculated using $(K_{2,incorect})Mg = (K_{2,ATP})Mg/(K_{2,ATP}/K_{2,incorrect})Mn$.

[c] k_{+3} in the presence of Mg^{2+} was calculated using eqs 3-5 under Experimental Procedures using the K_2 values listed above, the observed and maximal phosphorothioate effects listed in Table 2, and the k_{pol} values listed in Table 1.

NIH-PA Author Manuscript

NIH-PA Author Manuscript

NIH-PA Author Manuscript

Table 5

Kinetic Parameters for the Kinetic Mechanism of $3D^{pol}$-Catalyzed Nucleotide Incorporation in the Presence of Mn^{2+} (Scheme 1)

parameter	value[a]	K_{eq}
k_{+1}	10 μM^{-1} s^{-1}	
k_{-1}	40 s^{-1}	0.25 μM^{-1}
k_{+2}	300 s^{-1}	
k_{-2}	100 s^{-1}	3
k_{+3}	30 s^{-1}	
k_{-3}	22 s^{-1}	1.4
k_{+4}	≥160 s^{-1}	
k_{-4}	<0.0001 s^{-1}	$>1.6 \times 10_6$
k_{+5}	2000 s^{-1}	
k_{-5}	10 μM^{-1} s^{-1}	200 μM

[a] Values for all parameters, with the exception of k_{-3} and k_{-4}, were determined experimentally.

NIH-PA Author Manuscript

NIH-PA Author Manuscript

NIH-PA Author Manuscript

Table 6

Values for the Rate Constants Employed in Kinetic Simulations Are Constrained by Experimental Data[a]

experiment	2-fold change	10-fold change	insensitive
kinetics of AMP incorporation	k_{+1}, k_{-1},[b] k_{+2},[c] k_{-2},[b] k_{+3}	k_{+2}, k_{+4}[d]	k_{-3}, k_{-4}, k_{+5}, k_{-5}
pulse-chase analysis	k_{+2}, k_{+3}	k_{+1},[d] k_{-2}, k_{-3},[e] k_{+4}[d]	k_{-1}, k_{-4}, k_{+5}, k_{-5}
two-nucleotide incorporation (-PP_i)	k_{+1}, k_{+3},[c] $K_{d,app,UTP}$, $k_{pol,UTP}$	k_{-1},[e] k_{+2},[d] k_{-2},[e] k_{+3}, k_{-3},[e] k_{+4}[d]	k_{-4}, k_{+5}, k_{-5}
two-nucleotide incorporation (+PP_i)	k_{+1}, k_{+3}, k_{+5}, k_{-5}, $K_{d,app,UTP}$, $k_{pol,UTP}$	k_{-1}, k_{+2}, k_{-2},[e] k_{-3}[e]	k_{+4}, k_{-4}

[a] The rate constants shown in Table 5 were increased or decreased by 2- or 10-fold, and the fit of the simulation to the indicated experimental data was evaluated. In most instances, either an increase or decrease in the indicated rate constants altered the goodness of fit. However, exceptions were noted, and these are annotated to indicate this fact. Finally, rate constants that can be varied by greater than 10-fold without any apparent change in the fit of the simulation to the data are indicated in the column labeled insensitive.

[b] Only a 2-fold increase gives a significant change in the fit of the simulation to the data.

[c] Only a 2-fold decrease gives a significant change in the fit of the simulation to the data.

[d] Only a 10-fold decrease gives a significant change in the fit of the simulation to the data.

[e] Only a 10-fold increase gives a significant change in the fit of the simulation to the data.